# An investigation on the biodynamic foundation of a rat tail vibration model

**D E Welcome***, **K Krajnak, M L Kashon,** and **R G Dong**
Health Effects Laboratory Division, National Institute for Occupational Safety and Health, Morgantown, WV, USA

*The manuscript was received on 11 March 2008 and was accepted after revision for publication on 13 June 2008.*

DOI: 10.1243/09544119JEIM419

**Abstract:** The objectives of this study are to examine the fundamental characteristics of the biodynamic responses of a rat tail to vibration and to compare them with those of human fingers. Vibration transmission through tails exposed to three vibration magnitudes (1 *g*, 5 *g*, and 10 *g* r.m.s.) at six frequencies (32 Hz, 63 Hz, 125 Hz, 160 Hz, 250 Hz, and 500 Hz) was measured using a laser vibrometer. A mechanical-equivalent model of the tail was established on the basis of the transmissibility data, which was used to estimate the biodynamic deformation and vibration power absorption at several representative locations on the tail. They were compared with those derived from a mechanical-equivalent model of human fingers reported in the literature. This study found that, similar to human fingers, the biodynamic responses of the rat tail depends on the vibration magnitude, frequency, and measurement location. With the restraint method used in this study, the natural frequency of the rat tail is in the range 161–368 Hz, which is mostly within the general range of human finger resonant frequencies (100–350 Hz). However, the damping ratios of the rat tail at the unconstrained locations are from 0.094 to 0.394, which are lower than those of human fingers (0.708–0.725). Whereas the biodynamic responses of human fingers at frequencies lower than 100 Hz could be significantly influenced by the biodynamics of the entire hand–arm system, the rat tail biodynamic responses can be considered independent of the rat body in the frequency range used in this study. Based on these findings it is concluded that, although there are some differences between the frequency dependences of the biodynamic responses of the rat tail and human fingers, the rat tail model can provide a practical and reasonable approach to examine the relationships between the biodynamic and biological responses at midrange to high frequencies, and to understand the mechanisms underlying vibration-induced finger disorders.

**Keywords:** hand–arm vibration, rat tail model, biodynamic response, hand, fingers

## 1 INTRODUCTION

Occupational exposure to hand–arm vibration through the use of powered hand tools results in dysfunction of the peripheral vascular and sensory nervous systems in the hands and fingers that is collectively referred to as hand–arm vibration syndrome (HAVS) [**1**–**3**]. HAVS is typically characterized by a reduction in tactile sensation in the hands, a loss of grip strength and manual dexterity, and cold-induced blanching of the fingers and hands, which is referred to as vibration white finger (VWF) [**4**, **5**]. Studies performed on finger biopsy tissues collected from workers diagnosed with HAVS demonstrate that vibration exposure results in severe damage to the peripheral nerves, blood vessels, and skeletal muscles [**6**–**9**]. Although many of the physiological, biological, and structural changes correlated with HAVS have been characterized, understanding of how vibration induces these changes in soft tissues is far from complete.

Vibration transmission from a tool to the hand–arm system results in shear and compressive stresses and strains on exposed soft tissues that may result in structural damage to the exposed tissues and/or may

**Corresponding author: Health Effects Laboratory Division, National Institute of Occupational Safety and Health, 1095 Willowdale Road, MS L-2027, Morgantown, WV, 26505, USA. email: dwelcome@cdc.gov*

activate cellular processes that induce physiological dysfunction. A number of factors, such as the vibration frequency, vibration magnitude, duration, and grip force, can influence vibration transmission and the physical (i.e. biodynamic) responses of the exposed tissues to vibration [**10**]. Vibration frequencies and magnitudes that result in the greatest biodynamic response of the exposed tissue could pose a greater risk for injury or dysfunction [**10–12**]. However, the precise dose–response relationships between specific vibration-associated exposure factors and injury have not been determined. By understanding these dose–response relationships, more effective strategies for monitoring workers and preventing vibration-induced injuries could be developed.

Physiological and pathological mechanisms underlying vibration-induced injuries cannot be thoroughly examined in humans. Therefore, animal models have been developed to determine how vibration causes injury and dysfunction of the peripheral vascular and sensory systems. For example, exposing rats to hind limb or tail vibration has demonstrated that repeated exposures to vibration result in damage to vascular, neural, and muscle tissues [**13–17**]. The tissue damage seen in these rat models is similar to that seen in biopsy tissues collected from workers diagnosed with VWF [**6**, **7**]. Vascular and sensory changes that are induced by exposure to acute vibration are also similar in rats and humans [**16**, **18**, **19**]. Because the biological and physiological responses to acute and chronic vibration exposure are similar in rats and humans, it is likely that the aetiologies of these changes are similar too. Thus, rat models have been used to study the aetiology of vibration-induced injury. However, to understand fully the relationship between vibration exposure and injury, the biodynamic responses of tissues under different exposure conditions need to be characterized. To date, there has not been a systematic study of the biodynamic effects of vibration on any of the animal models that have been used.

The specific aims of this study were to understand the fundamental characteristics of the biodynamic responses of the rat tail in a typical experimental set-up. As mentioned above, the rat tail model is well established and has been used by a number of investigators to understand the mechanisms underlying vibration-induced injuries. In addition, because the rat tail lies away from the rest of the body, the biodynamic response of the tail can be easily assessed without causing much stress to the rat. These experiments specifically determined how vibration frequency and magnitude act independently and together to affect the biodynamic responses of the tail to vibration. Because the tail varies in thickness over its length, the vibration transmissibility was also examined as a function of location along the tail. A mechanical-equivalent model of a rat tail also was established on the basis of the transmissibility data and used to estimate the natural frequency and damping ratio of the tail, the dynamic deformation, and the vibration power absorption (VPA). Finally, as presented in section 4, these dynamic behaviours and properties were compared with the responses of a human finger reported in the published studies [**20–22**] or calculated from the recently reported model of the human fingers–hand–arm system [**23**].

## 2 METHODS

### 2.1 Animals

Four male Sprague–Dawley rats (Hla:(SD)CVF; 6 weeks of age; Hilltop Lab Animals, Inc., Scottsdale, Pennsylvania, USA) were used for the exposures. All procedures were approved by the Animal Care and Use Committee of the National Institute for Occupational Safety and Health and were in compliance with Public Health Service guidelines for the care and use of laboratory animals. The rats were placed in Broome-style restrainers for 4 h a day for 5 days to acclimatize them to restraint and to reduce the physiological effects of restraint stress. All rats were 7 weeks of age at the time of testing. The rats were allowed to walk into the restrainers, head first, and the tail was gently threaded through a hole in the removable hatch. The hole in the hatch had been enlarged so that the rats' tails were not held in an awkward position in relationship to their bodies. The rat's tail was gently placed on top of the platform and four elastic straps (6.35 mm wide) were pulled over the tail and fastened over screws secured into the side of the platform, as shown in Fig. 1. Care was taken to make sure that the tail was secured to the platform without compressing the tissue. At the beginning of the experiment, the rats had a mass of $273 \pm 4.3$ g (mean $\pm$ standard error of the mean). The dimensions of the rats' tails are listed in Table 1. All measurements were collected during a single exposure, and the rats were awake during the exposure.

### 2.2 Experimental Set-up

Because of the relative mass and size of the rat's tail compared with most commercially available accel-

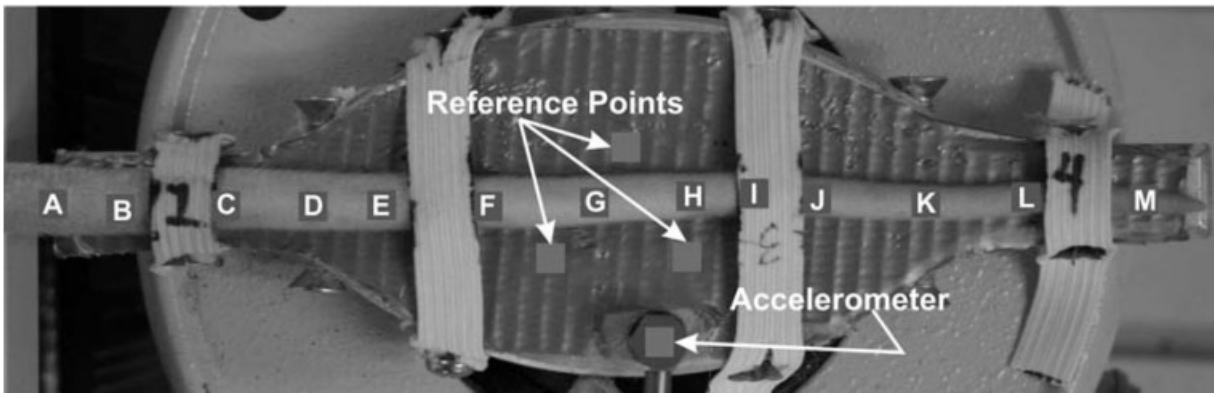


**Fig. 1** Map of the index locations on the tail and vibrating plate. Measurements were made at 13 points along the length of the tail as well as three reference points on the plate and one on the accelerometer

erometers, a non-contact method was used to assess the tail's transmissibility. Vibration-induced motion at specific points along the length of the tail was measured using a scanning laser vibrometer (Polytec PSV-300-H). Figure 2 shows a schematic diagram of the experimental test set-up. The vibrometer was placed over the tail, which rested on a vertically oscillating shaker platform centred directly behind the restrained rat. The input vibration was generated by a V408 electromagnetic shaker and PA100E power amplifier combination (both from Ling Dynamic Systems) driven by a Prema function generator and the laser vibrometer's control software (Polytec version 8.2). The input acceleration of the platform was monitored via an accelerometer (PCB 353B15) fed into a data acquisition and analyser system (B&K Type 3032A input–output module, pulse version 6.0).

The shaker platform was a flat aluminium ellipse, 50 mm × 25 mm (major and minor radii respectively), which was 12.7 mm thick, tapered to 6.35 mm at the ends, and had 14 mm wide extensions to lengthen the entire platform from the middle ellipse to 170 mm. This shape was chosen to minimize the mass and bending response of the platform, thus maintaining a high resonant frequency while accommodating the screw attachments to the shaker, a variety of tail constraint methods, the length and growth of the rat's tail, and the accelerometer.

**Table 1** Lengths and diameters of the rats' tails

| Rat | Tail length (mm) | Diameter at a quarter rostral (mm) | Diameter at mid length (mm) | Diameter at a quarter caudal (mm) |
|---|---|---|---|---|
| 3 | 192.0 | 9.5 | 6.0 | 3.0 |
| 4 | 197.0 | 8.0 | 5.0 | 3.0 |
| 5 | 194.0 | 6.0 | 5.0 | 3.0 |
| 6 | 190.5 | 8.0 | 5.0 | 3.0 |

The platform showed a flat uniform response with minimal bending to 800 Hz. The effects of frequency were tested up to 500 Hz in the present study. The maximum vibration difference across the platform was less than 5 per cent, which is conventionally accepted for many practical engineering applications. The top surface of the platform was covered with a layer of duct tape to improve its reflectivity to the laser and to decrease heat losses (from the tail) for the rat.

### 2.3 Test conditions and study variables

Discrete sinusoidal vibrations at six different frequencies (32 Hz, 63 Hz, 125 Hz, 160 Hz, 250 Hz, and 500 Hz) and each of three constant accelerations (1 *g*, 5 *g*, and 10 *g* r.m.s.) were used for the exposures. The frequencies are third-octave band frequencies in ranges typical of the dominant frequencies for many tools such as chipper and rivet hammers at the low-end and high-cycle grinders and saws in the higher end of the frequency range. Preliminary testing using periodic chirp signals indicated peak amplification between 160 and 200 Hz for the middle of the tail.

The velocity was measured for an array of 13 index points on the tail and four reference points (three on the plate and one on the accelerometer (Fig. 1)). Index points A and B generally corresponded to portions of the tail around the C3 and C4 vertebrae, points C to E corresponded to the C7 to C9 vertebrae, points F to H corresponded to the C12 to C15 vertebrae, points J to L corresponded to the C18 to C21 vertebrae, and point M corresponded to vertebrate C25 or C26. The accelerations at each point for each test were calculated via the vibrometer software (Polytec PSV 8.2). The transmissibility $T_r$ was then

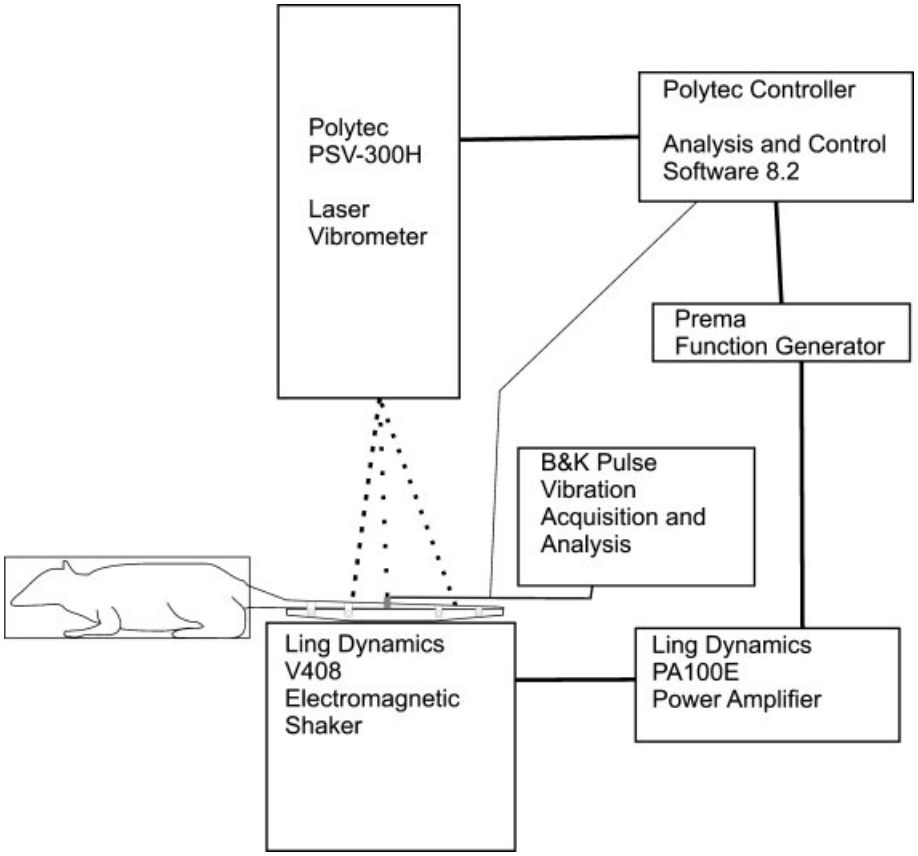


**Fig. 2** Schematic diagram of the equipment set-up used for measuring the rat tail transmissibility

calculated for each tail point in each trial using

$$T_r = \frac{|A_i|}{|A_{ref}|} \quad (1)$$

where $A_i$ represents the output acceleration at each index $i$ on the tail and $A_{ref}$ is the average response of the reference points. The coefficient of variation among the reference points was generally below 1 per cent, although it ranged from 1 per cent to 3.5 per cent at 125 and 160 Hz, still indicating a uniform input across the plate. The laser (sampling speed, 10 m/s) had a sensitivity of 25 mm/s and the frequency analyser was set to analyse 1600 lines sampled at 1600 Hz for the 500 Hz input and 800 lines at 800 Hz for the others.

### 2.4 Statistical analysis

Transmissibility data were analysed using SAS/STAT software, Version 9.1, of the SAS System for Windows (SAS Institute, Cary, North Carolina, USA). A mixed model three-factor within-subject analysis of variance (ANOVA) was used to conduct the initial statistical analysis. The design factors included index point location, vibration frequency, and vibration magnitude. All treatment combinations were assessed in each rat and the animal was included in the statistical model as a random effect to model appropriately the covariance structure reflecting the repeated measures within an animal. As there was a significant three-way interaction among the factors, subsequent two-way mixed model ANOVAs were generated at each index location to determine the specific effects of the vibration frequency and vibration magnitude in a stratified fashion. *Post-hoc* comparisons were also carried out using Fisher's least-significant-difference method. All differences and effects were considered significant at $p < 0.05$.

### 2.5 Mechanical-equivalent model of the rat tail

The biodynamic deformation of the rat tail referred to in this study is defined as the displacement of the tail relative to its contact surface in the vibration direction. Similar to finger strain [**24**], the deforma-

tion can be used as an approximate measure of the average strain inside the tail. Another important biodynamic measure is VPA, which is defined as the dynamic force multiplied by the vibration velocity [**25**]. Because the total VPA in a structure can be integrated from the product of the biodynamic stress and the strain rate distributed in the structure, the VPA is a combined measure of both stress and strain rate. Thus, it has been hypothesized that the VPA distributed in a structure is related to the aetiology of the vibration-induced physiological and pathological effects in the local structures [**23**, **25**]. As an essential step to test this hypothesis using the rat tail model, it is necessary to quantify the distributed VPA and biodynamic strain in the tail. To date, no method for the direct measurement of these variables is available, and a reliable finite element model for their accurate prediction has not been developed. As the first degree of approximation, both the deformation and the VPA of the tail were estimated in this study using a mechanical-equivalent model that was established on the basis of the measured transmissibility. Such a model was also required to estimate the natural frequency and damping ratios of the rats' tails.

The measured transmissibility data reveal that the response of the tail at each measurement point approximately follows the dynamic response pattern of a one-degree-of-freedom (1DOF) mechanical structure, as presented in section 3. This observation suggests that the rat tail is flexible and the tail's vibration motion is almost independent of the rat's body in the frequency range used in this study. Therefore, to simplify the problem, the tail was conceptually divided into several sections, with each section centred at the point for the transmissibility measurement. The mass, stiffness, and damping were assumed to be uniformly distributed along the length of the tail in each section. The unit length of the tail in each section was simulated using a 1DOF mechanical-equivalent model, as shown in Fig. 3. The moving effective mass $M_{\text{Tail}}$ in the mechanical model was assumed to be the tail mass per unit length. To determine the effective mass at each measurement location, the mass, length, and cross-sectional areas of each tail were measured at three locations C, G, and K, and a conical shape of the tail was assumed. The tail effective mass is connected to the vibrating surface using a linear effective contact stiffness $k_{\text{Tail}}$ and viscous damping (per unit length) $c_{\text{Tail}}$. The measured vibration transmissibility was used to determine the stiffness and damping of the rat tail model using a conventional least r.m.s.

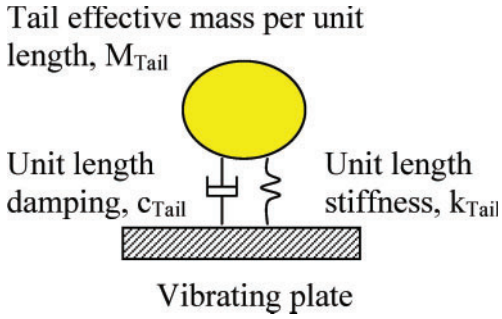


**Fig. 3** A mechanical-equivalent model of the rat tail

method, minimizing the r.m.s. difference between the modelling prediction and the measured transmissibility data. After the model parameters for the tail model at each location were determined, the relative displacement $\Delta D_{\text{Tail}}$ between tail's equivalent mass and the vibrating plate for each of the three input accelerations (1 *g*, 5 *g*, and 10 *g* r.m.s.) was calculated using the model shown in Fig. 3 and utilized to represent the overall deformation of the tail.

With the deformation, the power $P_{\text{Tail}}$ absorbed in each unit length of the tail was calculated from

$$P_{\text{Tail}}(\omega) = c_{\text{Tail}}[\omega\ \Delta D_{\text{Tail}}(\omega)]^2 \tag{2}$$

where $\omega$ is the vibration frequency in radians per second and $\Delta D_{\text{Tail}}$ is the r.m.s. value.

A method has been developed to estimate the total human finger VPA [**23**]. However, a method for estimating the power per unit length of each finger has not been developed. The unit tail VPA is not directly comparable with the total finger VPA. It is also inappropriate to compare directly the total VPA of the entire rat tail with the total VPA of an entire finger because the total volumes of tissues involved in the VPA are different. This is also unnecessary if the major concern is to compare the frequency dependences of the tail and finger VPAs. The best approach for comparing their frequency dependences is to derive their frequency weightings. A general method for the derivation has been developed from a previous study [**26**]. Applying it to this study, the tail VPA weighting $W_{\text{Tail}}$ for each of the three input accelerations (1 *g*, 5 *g*, and 10 *g* r.m.s.) was derived from the formula

$$W_{\text{Tail}}(\omega) = \sqrt{\frac{P_{\text{Tail}}}{P_{\text{Tail\_Ref}}}} = \frac{\omega\ \Delta D_{\text{Tail}}(\omega)}{\omega_{\text{Ref}}\ \Delta D_{\text{Tail\_Ref}}(\omega_{\text{Ref}})} \sqrt{\frac{c_{\text{Tail}}}{c_{\text{Tail\_Ref}}}} \tag{3}$$

where $P_{\text{Tail\_Ref}}$ is the reference VPA value that can be selected on the basis of the convenience of the comparison with the finger VPA weighting.

## 3 RESULTS

### 3.1 Inter-animal variability

The graphs in Fig. 4 depict the frequency-dependent transmission of vibration along the length of each rat's tail at 5 *g*. The location-dependent responses of the tail at each vibration frequency and magnitude were similar in all rats. Variance estimates from the ANOVA revealed that 9.8 per cent of the total variance was due to differences between rats, and thus approximately 90 per cent of the variance was the result of the exposure. Responses and variability at 1 *g* and 10 *g* were similar to responses at 5 *g*. All results that follow are based on the mean response of all four rats.

### 3.2 Vibration-frequency-dependent effects

Figure 5 shows the mean transmissibility at each location for each vibration frequency and input

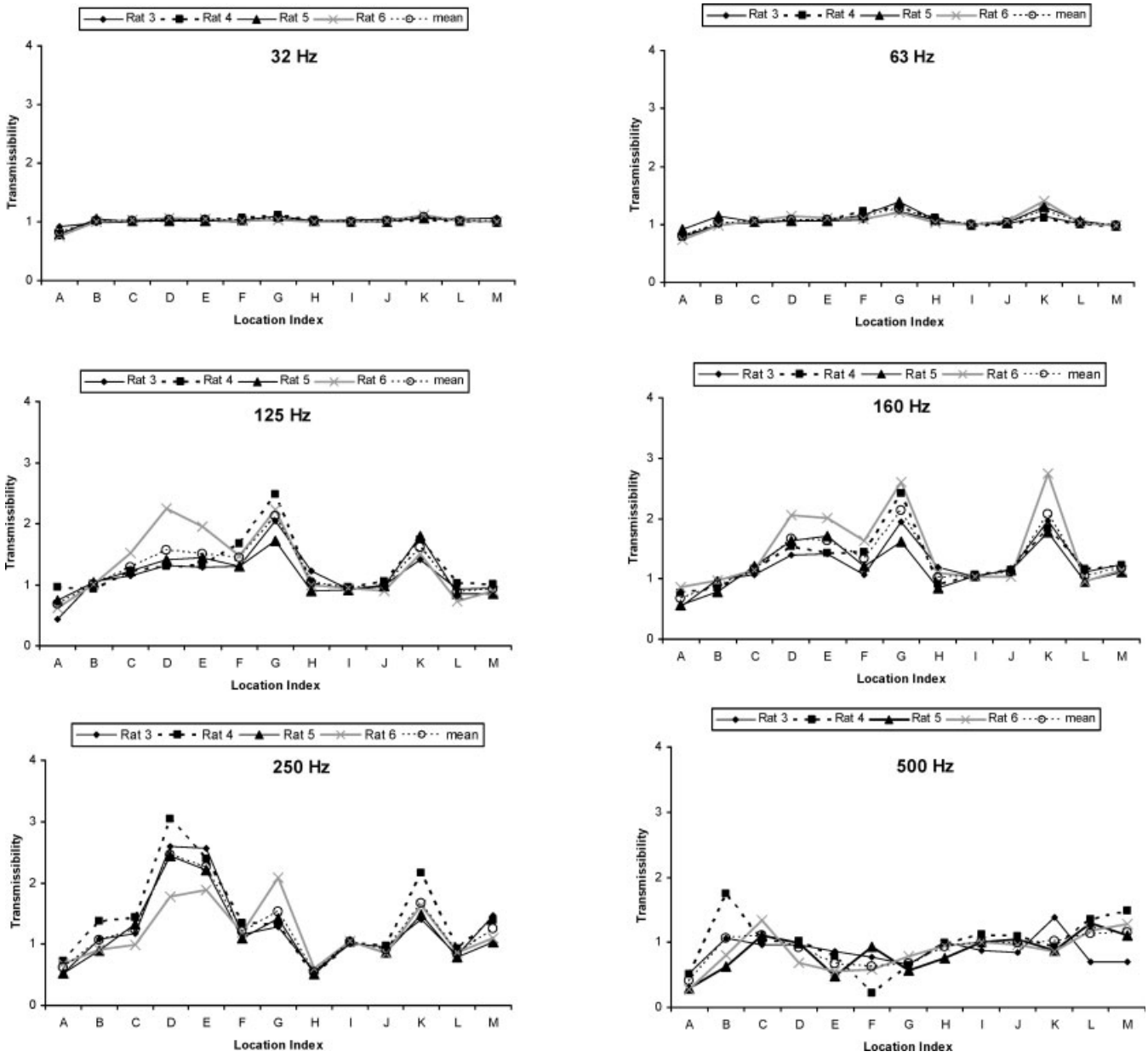


**Fig. 4** Transmissibility among the rats for a 5 *g* r.m.s. excitation for 32 Hz, 63 Hz, 125 Hz, 160 Hz, 250 Hz, and 500 Hz

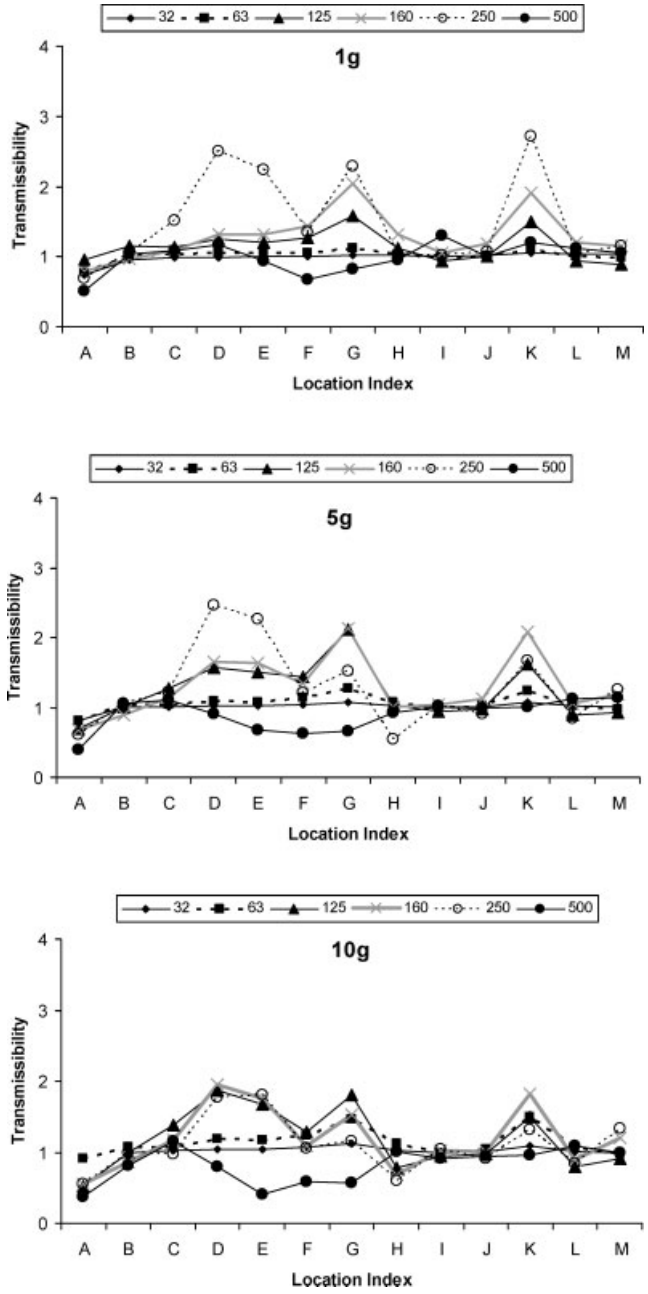


**Fig. 5** Comparisons of the transmissibility at each frequency by location for 1 *g*, 5 *g*, and 10 *g*

magnitude. Analysis of these data resulted in a significant three-way interaction ($p < 0.0001$). Examining the effects of frequency on transmissibility demonstrated that transmissibility was near unity at all locations along the length of the tail at 32 Hz and 63 Hz (Fig. 5). Vibration exposure from 125 to 250 Hz resulted in an increase in transmissibility which was greatest at the midpoints between the straps (e.g. areas D, G, and K; $p < 0.01$). Regions near the restraint straps (e.g. C, E, and F) also displayed significant increases in transmissibility at exposures of 125–250 Hz ($p < 0.05$); however, these increases were generally smaller than those seen at the midpoints. At 500 Hz, transmissibility remained at unity or was damped. Transmissibility generally remained near unity in strapped regions and at the most proximal portion of the tails (regions A and B) at all exposure frequencies.

### 3.3 Vibration-magnitude effects

Figure 6 shows the frequency-dependent responses at the three different vibration magnitudes at six points on the tails (i.e. C, D, E, F, G, and K). In the unstrapped regions of the tail and in the regions near the straps, the analyses identified significant frequency by magnitude interactions ($p < 0.01$). In these regions of the tail, transmissibility is generally significantly greater at 1 *g* than at 5 *g* or 10 *g* ($p < 0.05$). In addition, the resonant peaks tended to shift to lower frequencies as the overall transmissibility lessened at the higher vibration magnitude exposures.

### 3.4 Modelling results

Figure 6 also demonstrates that the proposed mechanical-equivalent model of the rat tail fits the experimental data reasonably well. Thus, the mechanical-equivalent model was used to calculate the resonant frequencies and damping ratios at the six different locations shown in Fig. 6. These values are listed in Table 2. The results indicate that the resonant frequency generally decreases with increases in the vibration magnitude. However, the damping ratio increases with increases in the vibration magnitude. In addition, the damping ratios at the strapped locations (e.g. C and F) are greater than those at points between the straps (e.g. D, G, and K).

Figure 7 shows the calculated dynamic deformation of the rat tail at the six locations. The basic shapes of the deformation are similar to those of their corresponding transmissibility functions shown in Fig. 6. Obviously, increasing the vibration magnitude increases the deformation. The resonant deformations at the strapped points (e.g. C and F) are lower than those at the unconstrained points.

Figure 8 shows the rat tail VPA per unit tail length (metre) at the same six locations calculated from equation (2). Each tail VPA also generally reaches its peak value at the resonant frequency identified from the mechanical-equivalent model. Because the damping ratios at the strapped points are generally larger than those at the unconstrained points (see Table 2), the relative positions of the VPA

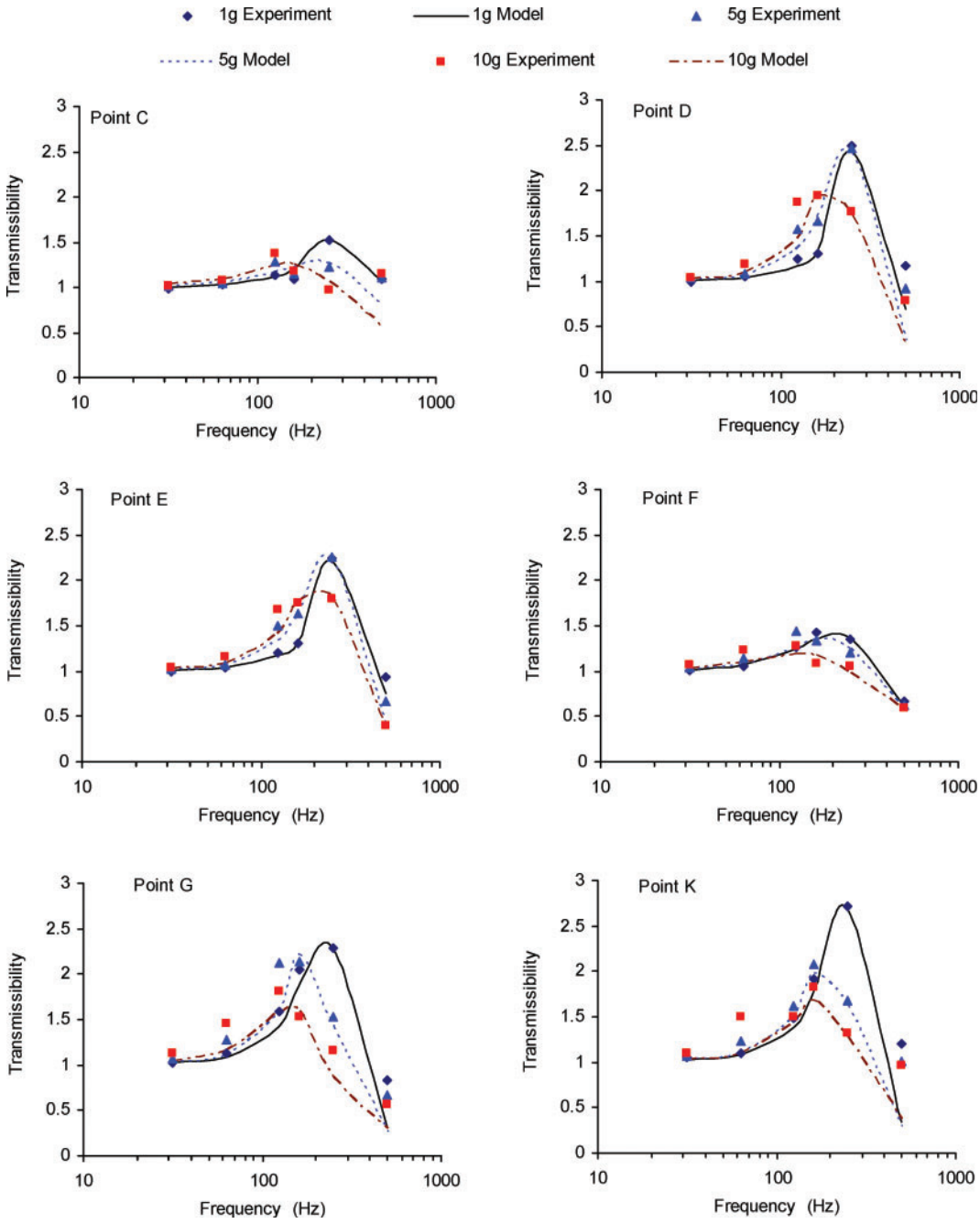


**Fig. 6** Frequency responses at six locations (C, D, E, F, G, and K) and modelling results

values among the six locations are different from the transmissibility curves and the deformation curves. However, the peak values of the tail VPA at the unconstrained points remain at the highest level.

## 4 DISCUSSION

This study used vibration transmissibility to characterize the frequency-, magnitude-, and location-dependent biodynamic responses of rats' tails to sinusoidal vibration. In general, it was demonstrated that the biodynamic response of the tail was location dependent and that the location-dependent pattern of transmissibility was affected by the vibration frequency. Changing the vibration magnitude also affected transmissibility by shifting the resonant frequencies and altering the amplitude of the transmissibility. Based on these results, it was concluded that the rat tail model can be used to examine the frequency- and magnitude-dependent responses of soft tissues to vibration exposure.

**Table 2** Natural frequencies and damping ratios for six measurement locations (C, D, E, F, G, and K) under three excitation magnitudes (1 *g*, 5 *g*, and 10 *g*), calculated from the rat tail mechanical-equivalent model (Fig. 3). The model parameters were determined from the measured vibration transmissibility at each of the six locations

| Measured location | Vibration input (units of *g*) | Natural frequency (Hz) | Damping ratio |
|---|---|---|---|
| C | 1 | 368 | 0.366 |
| | 5 | 278 | 0.692 |
| | 10 | 193 | 0.721 |
| D | 1 | 319 | 0.094 |
| | 5 | 235 | 0.202 |
| | 10 | 212 | 0.219 |
| E | 1 | 324 | 0.147 |
| | 5 | 241 | 0.236 |
| | 10 | 221 | 0.253 |
| F | 1 | 245 | 0.523 |
| | 5 | 224 | 0.58 |
| | 10 | 172 | 0.872 |
| G | 1 | 223 | 0.174 |
| | 5 | 198 | 0.202 |
| | 10 | 161 | 0.394 |
| K | 1 | 233 | 0.17 |
| | 5 | 208 | 0.224 |
| | 10 | 201 | 0.365 |

### 4.1 Effects of vibration frequency and magnitude on transmissibility

Transmissibility in rats' tails gradually increased with increases in frequency before reaching the resonant peak but dramatically declined with increases in frequency beyond peak resonance. The resonant frequencies of rat tails using our restraint and exposure system were in the range 161–368 Hz, depending on the location of the measurement and the magnitude of the input. The resonant frequency decreased as the vibration magnitude increased. The range of resonant frequencies displayed by the rat tail is similar to the resonant frequencies measured in human fingers. Figure 9 shows several typical sets of transmissibility data in the human fingers collected in experiments [**21**, **22**], or by prediction using the five-degrees-of-freedom (5DOF) model shown in Fig. 10 [**23**]. The experimental data were measured at the middle phalanx [**21**, **22**], which may be considered as the average transmissibility of the fingers. The predicted data also represent the overall response of the fingers [**23**]. In these studies, the resonant frequencies were in the range 100–350 Hz. The influence of vibration magnitude on finger resonance has not been reported. However, increasing the vibration magnitude reduces the resonant frequency of the entire hand–arm system [**21**]. Therefore, it is likely that increases in magnitude reduce the natural frequency in fingers, as it does in rats' tails.

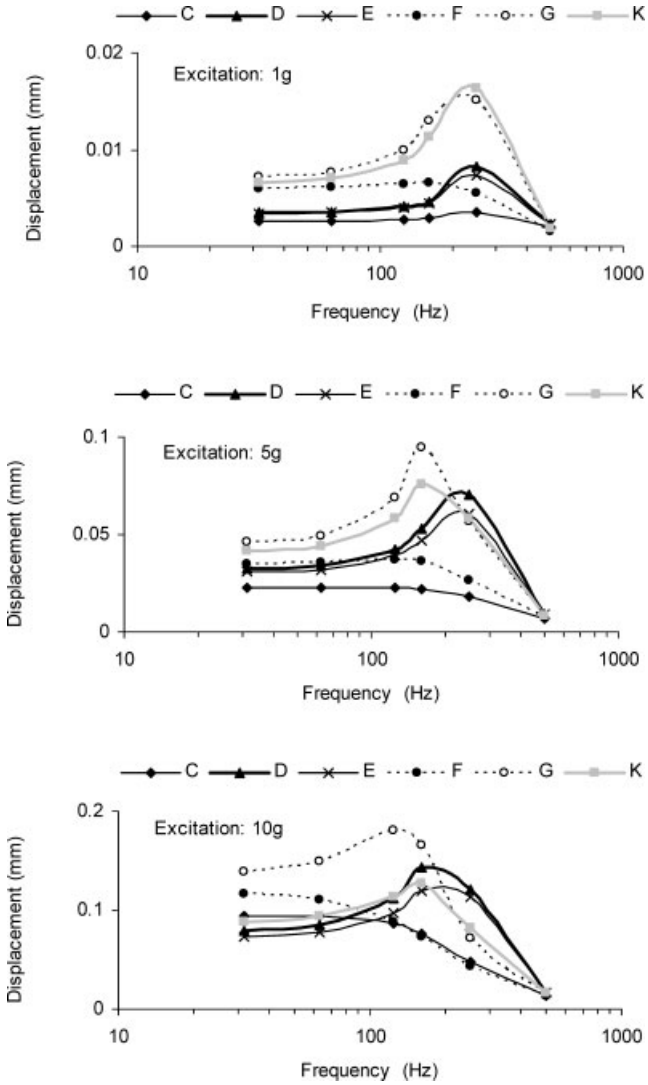


**Fig. 7** Rat tail dynamic deformation at six locations (C, D, E, F, G, and K)

The major difference between the transmissibility functions of the fingers (Fig. 9) and the rat tail (Fig. 6) is that the rat tail generally has a sharper resonant peak, especially in the unrestrained locations (e.g. points D, G, and K). This is because damping is generally lower in the tail than in the fingers. The damping ratios in the rats' tails were between 0.094 and 0.394 (Table 2), depending on the location and magnitude of the exposure. In contrast, damping ratios in the human fingers calculated from the hand–arm system model are in the range 0.708–0.725 [**23**]. The damping ratios in the strapped regions of the tail (e.g. points C and F) are more comparable with the ratios calculated for the fingers.

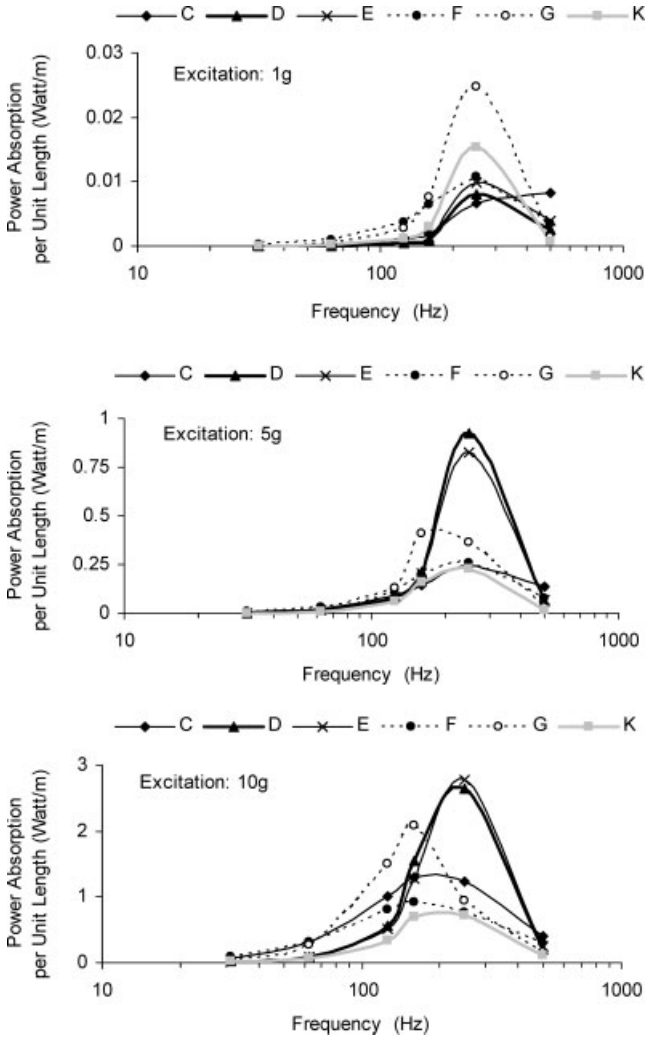


**Fig. 8** Rat tail vibration power absorption intensity at six locations (C, D, E, F, G, and K)

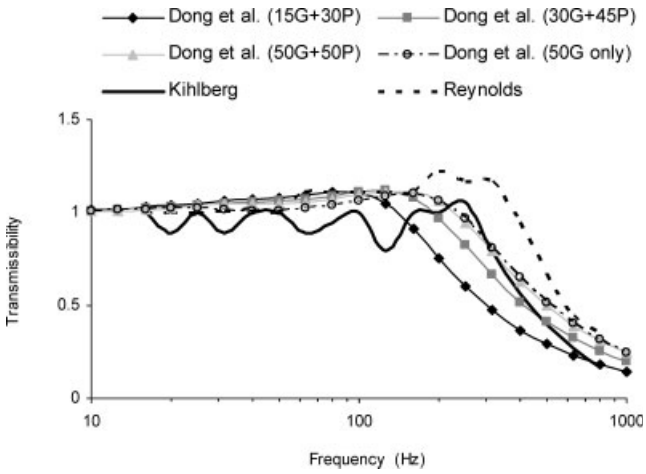


**Fig. 9** Comparisons of the human finger's vibration transmissibility. Data from references [**21**] and [**22**] and the modelling transmissibility values were calculated using the models reported by Dong *et al.* [**23**] collected with the grip (G) and push (P) forces noted in the key

### 4.2 Dynamic deformation comparison

In human fingers, dynamic deformation is affected by the fingers-applied force. Figure 11 shows the finger dynamic deformations calculated from the model reported in reference [**23**], together with those of the rat tail at six measurement locations. Reducing the fingers-applied force generally increases the finger dynamic deformation because the finger contact stiffness decreases with the reduction in the contact force. A similar relationship between contact force and dynamic deformation is seen in rats' tails. Dynamic deformation of tails was calculated using the transmissibility data and the tail model. At the unrestrained locations (e.g. points D, G, and K), where the tail contact forces were lower, deformation was high whereas, at the restrained locations where contact forces were higher, deformation was lower (e.g. points C and F). Thus, as contact force is increased in either the finger or the tail, dynamic deformation is reduced.

A number of other factors also influence dynamic deformation. For example, increasing the source vibration magnitude increases deformation in both the fingers and the tail. However, at the same vibration magnitude levels, finger dynamic deformation is higher than tail deformation at frequencies less than 63 Hz, and somewhat lower than the unrestrained portions of the tail at frequencies greater than 100 Hz. One factor accounting for the differences in dynamic deformation between the tail and fingers is that the rat's tail is highly flexible and the biodynamic response is almost independent of the rat's body. In contrast, the responses of the fingers are generally affected by the response of the whole hand–arm system, particularly at lower frequencies. However, the finger responses become more independent of the remaining hand–arm system as the vibration frequency increases [**23**, **25**]. Therefore, the finger deformation responses at higher frequencies are more comparable with those of the rat tail because more proximal body regions are not mediating the local responses to vibration at these frequencies. Studies using the rat model to determine the biological effects of vibration on physiology have used a range of vibration frequencies; however, the majority of these studies have focused on the effects of exposure frequencies around 60 Hz (see, for example, reference [**16**]). Future studies also should examine the biological responses at higher frequencies where there is greater tissue

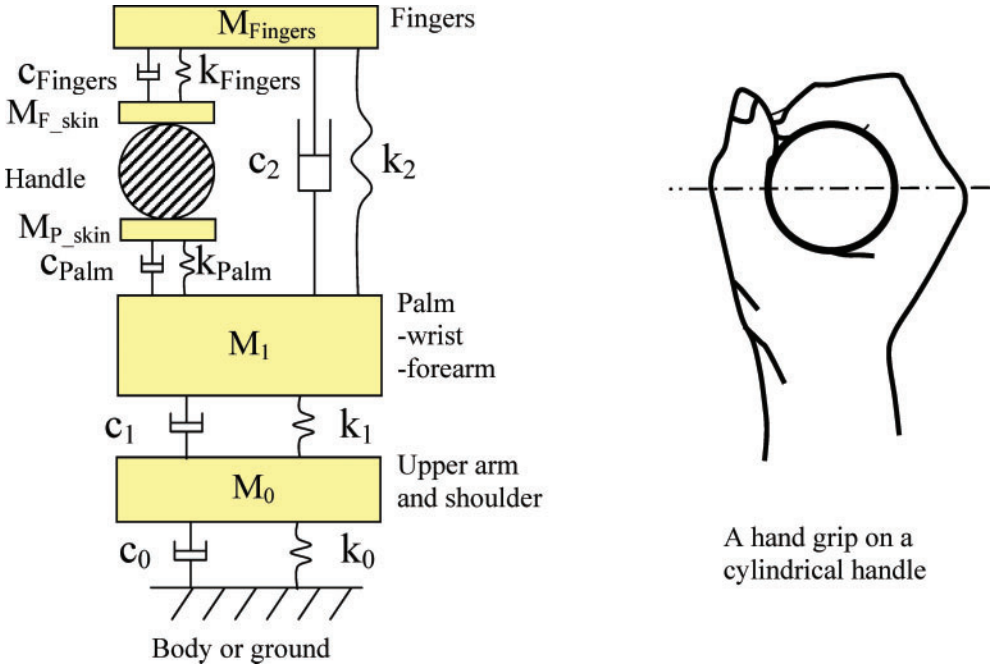


**Fig. 10** A 5DOF mechanical-equivalent model of the human fingers–hand–arm system [**23**]

deformation, and the biodynamic response is more similar to the responses seen in human fingers.

Another factor influencing tissue deformation and strain is the cross-sectional area of the exposed region of the body. The maximum strain induced by a given deformation theoretically increases with the reduction in the cross-sectional effective radius of the appendage that is in contact with the vibrating plate or the tool handle. If maximum strain is the dominant controlling factor in developing an injury, the comparable strain frequency range may be broader in humans and include frequencies at lower ranges than the rat tail. This is because the radius of the tail is usually less than that of a human finger and the larger deformation found on a human finger at low frequencies could be compensated by its larger contact radius. Finite element models of the tail and finger can be developed to determine the detailed strain deformation distribution and the maximum strain, which may provide a better estimation of strain–frequency ranges. However, the results of this study suggest that the higher tail deformation in the resonant frequency range and the smaller tail radius are likely to result in a relatively higher maximum strain inside the tail.

The higher dynamic deformation of the rat tail than the fingers in the resonant frequency range occurs primarily because the tail has less damping than the fingers, especially at the unrestrained locations (e.g. D, G, and K). The results of this study suggest that the restraint strap increases the damping effect and reduces the resonance. A system could be developed to restrain the whole tail. This system would increase the damping ratio and result in a vibration-induced deformation response that is more comparable with that seen in humans. Increasing the restrained area and the applied static force will also reduce the resonant frequency of the tail. By comparing the results of the two different tail restraint systems, injury induced by greater deformation can be compared with injury induced by an increased static load. Studies in humans have demonstrated that solely increasing the static load can affect various physiological processes such as blood flow [**27**, **28**]. Determining how vibration and static load affect these physiological parameters is critical because both these factors may influence the risk of hand–arm injury in workers.

### 4.3 Power absorption comparison

Figure 12 shows the finger VPA frequency weighting functions for the four hand actions calculated using the model shown in Fig. 10 [**23**], together with those calculated from equation (3) for the tail at the six identified locations. They are normalized to the maximum finger power absorption and the maximum tail power absorption respectively. The finger VPA remains fairly flat in a large frequency range but the tail VPA weighting changes dramatically with the variation in frequency. Therefore, their basic trends

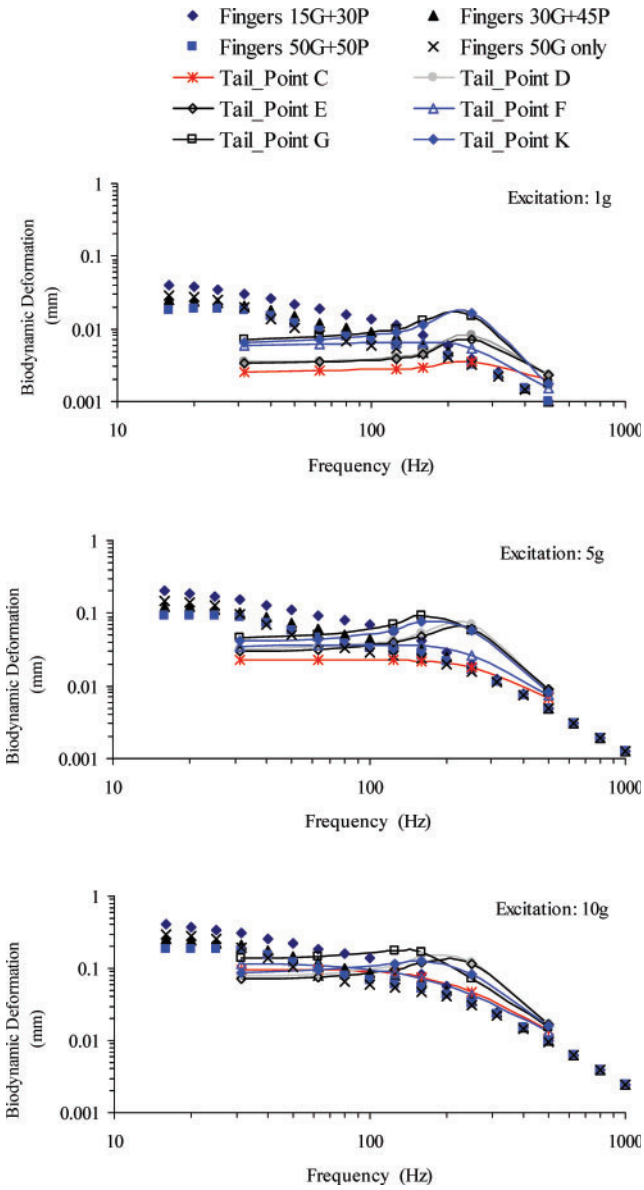


**Fig. 11** Dynamic deformation of human fingers calculated using the models reported by Dong *et al.* [**23**]

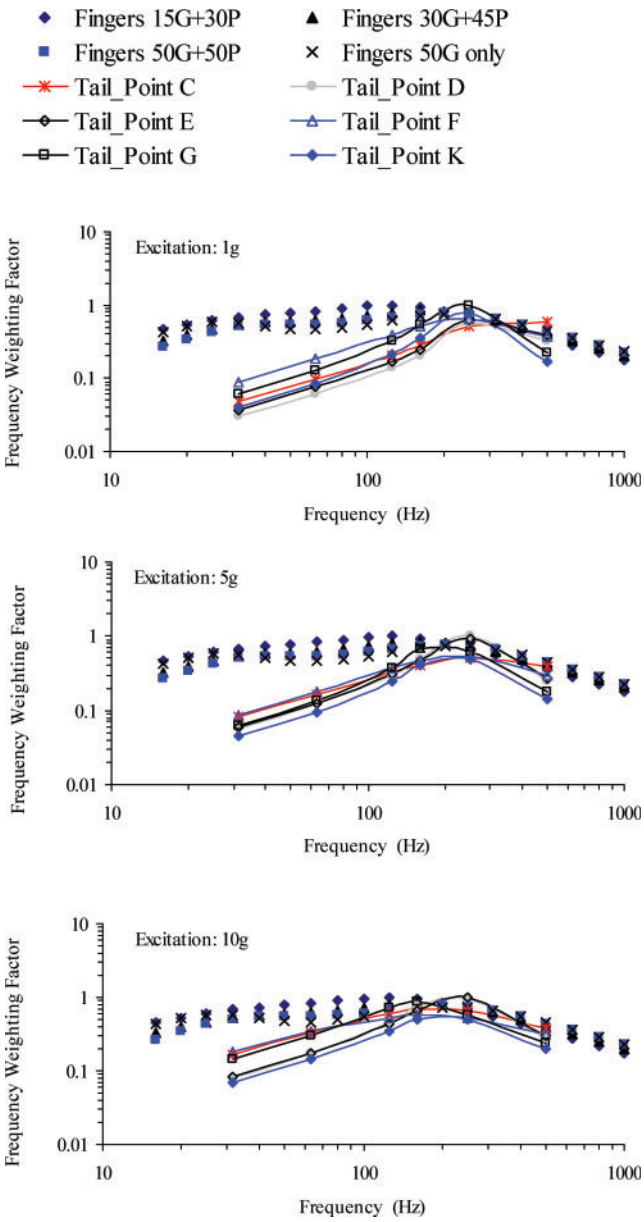


**Fig. 12** Vibration power absorption of human fingers calculated using the models reported by Dong *et al.* [**23**]

are very different. The highest tail VPA weighting remains in the neighbourhood of the tail's resonant frequency. The other observations are similar to those shown in the deformation comparison.

### 4.4 Major limitations

The effects of vibration magnitude on transmissibility clearly indicate that the rat tail model is a non-linear system. The significant interactions between the measurement location and the vibration magnitude and frequency also suggest that the rat tail is a continuous system in which the responses at one point could affect those at other points. Besides gravity, a large part of the restraint of the rat tail is provided by the straps. The unstrapped locations are indirectly affected by the straps through the tail's shear and tension stiffness, and damping. At high vibration magnitudes (e.g. 10 *g*), the unrestrained portions of the tail may lose contact with the vibration platform. This may reduce the effective contact stiffness and it explains why the resonant frequency decreases with the increase in the vibration magnitude. Therefore, the detailed biodynamic responses of the rat tail could be very complex. It is

impossible to use the 1DOF mechanical-equivalent model to simulate accurately the responses and the detailed interaction mechanisms. However, part of the non-linear behaviours is actually taken into account in the modelling by determining the specific model parameters for each location under each vibration magnitude. The major errors may also be estimated from the differences between the modelling results and the experimental data shown in Fig. 6. Because the trends or patterns of the modelling results are consistent with the transmissibility experimental data, it is acceptable to use the model to identify trends of the frequency dependences of the rat tail biodynamic responses. To obtain a more comprehensive understanding of the biodynamic responses of the rat tail, future studies may quantify the static and dynamic contact forces at various locations of the tail, in addition to the measurement of the vibration transmissibility using the laser vibrometer. A non-linear finite element model of the tail can also be developed to determine the detailed biodynamic response inside the tail.

Although the general effects of frequency on transmissibility and the ranges of resonant frequencies are similar in rats' tails and human fingers, the rat tail model cannot be used to study all aspects of frequency on transmissibility. For example, increasing the applied finger force increases the resonant frequency of the fingers [**23**]. Although the contact force between the vibration plate and tail could be artificially increased in the model, it would not be the same as increasing the force in the human hand system, where muscles are contracted and hand posture may be altered to maintain changes in force. Even with these limitations, the results from this study demonstrate that the rat tail model can be used to understand the effects of vibration frequency and magnitude on soft tissues and to characterize the relationship between the biodynamic responses of exposed tissues and the risk of injury.

## 5 CONCLUSIONS

This study found that the vibration magnitude, frequency, and location affect the biodynamic responses of the rat's tail. With the restraint method used in this study, the natural frequency of the rat tail is in the range 161–368 Hz, which is mostly within the general range of human finger resonant frequencies (100–350 Hz). However, the damping ratios of the rat tail at the unconstrained locations are much lower than that of human fingers. Whereas the biodynamic responses of human fingers at frequencies lower than 100 Hz could be significantly influenced by the biodynamics of the entire hand–arm system [**20**], the biodynamic responses of the rat tail at the excitation frequencies used in this study can be considered independent of the rat's body because of the tail's large flexibility. Because of these differences, the biodynamic responses under the same vibration magnitude in the tail exposed to frequencies lower than a certain value (e.g. less than 63 Hz) could be less than those of the human fingers. In the ranges of the tail's resonant frequency, the tail's responses are comparable with or somewhat higher than those of the human fingers, and thus injury development may be accelerated in the rat at these frequencies. These observations suggest that the basic trends of the biodynamic responses of the rat tail and human fingers display some differences in the major frequency range of concern in the hand-transmitted vibration exposure. These differences must be taken into account if data regarding the frequency dependent effects of vibration on vascular and neural physiology are to be used to determine the risk of developing vibration-induced finger disorders. The results of this study also suggest that the rat tail model can be used to investigate the relationships between the biodynamic and biological responses, which are important for understanding the mechanisms underlying the development of the vibration-induced finger disorders.

## ACKNOWLEDGEMENTS

The content of this publication does not necessarily reflect the views or policies of the NIOSH, nor does mention of trade names, commercial products, or organizations imply endorsement by the US Government.

## REFERENCES

1 **Bernard, B. P., Putz-Anderson, V., Burt, S. E., Cole, L. L., Fairfield-Estill, C., Fine, L. J., Grant, K. A., Gjessing, C., Jenkins, L., Hurrell, J. J., Nelson, N., Pfirman, D., Roberts, R. L., Stetson, D., Haring-Sweeney, M.,** and **Tanaka, S.** Musculoskeletal disorders and workplace factors. A critical review of epidemiologic evidence for work-related musculoskeletal disorders of the neck, upper extremity, and low back. Report, NIOSH, Cincinnati, Ohio, USA, 1997, p. 400.

2 **Friden, J.** Vibration damage to the hand: clinical presentation, prognosis and length and severity of vibration required. *J. Hand Surg. Br.*, 2001, **26**(5), 471–474.

3 **Griffin, M. J.** *Handbook of human vibration*, 1990 (Academic Press, San Diego, California).

4 **Stoyneva, Z., Lyapina, M., Tzvetkov, D.,** and **Vodenicharov, E.** Current pathophysiological views on vibration-induced Raynaud's phenomenon. *Cardiovascular Res.*, 2003, **57**(3), 615–624.

5 **Palmer, K. T., Griffin, M. J., Syddall, H., Pannett, B., Cooper, C.,** and **Coggon, D.** Prevalence of Raynaud's phenomenon in Great Britain and its relation to hand transmitted vibration: a national postal survey. *Occup. Environ. Medicine*, 2000, **57**(7), 448–452.

6 **Takeuchi, T., Futatsuka, M., Imanishi, H.,** and **Yamada, S.** Pathological changes observed in the finger biopsy of patients with vibration-induced white finger. *Scand. J. Work, Environment Health*, 1986, **12**(4), 280–283.

7 **Takeuchi, T., Takeya, M.,** and **Imanishi, H.** Ultrastructural changes in peripheral nerves of the fingers of three vibration-exposed persons with Raynaud's phenomenon. *Scand. J. Work, Environment Health*, 1988, **14**(1), 31–35.

8 **Goldsmith, P. C., Molina, F. A., Bunker, C. B., Terenghi, G., Leslie, T. A., Fowler, C. J., Polak, J. M.,** and **Dowd, P. M.** Cutaneous nerve fibre depletion in vibration white finger. *J. R. Soc. Medicine*, 1994, **87**(7), 377–381.

9 **Necking, L. E., Lundborg, G., Lundstrom, R., Thornell, L. E.,** and **Friden, J.** Hand muscle pathology after long-term vibration exposure. *J. Hand Surg. Br.*, 2004, **29**(5), 431–437.

10 **Dong, R. G., Wu, J. Z.,** and **Welcome, D. E.** Recent advances in biodynamics of human hand–arm system. *Ind. Health*, 2005, **43**(3), 449–471.

11 **Bovenzi, M.** Exposure–response relationship in the hand–arm vibration syndrome: an overview of current epidemiology research. *Int. Arch. Occup. Environ. Health*, 1998, **71**(8), 509–519.

12 **Bovenzi, M., Lindsell, C. J.,** and **Griffin, M. J.** Response of finger circulation to energy equivalent combinations of magnitude and duration of vibration. *Occup. Environ. Medicine*, 2001, **58**(3), 185–193.

13 **Hellstrom, B.** Effects of local vibration on the rat tail circulation. *Int. Arch. Arbeitsmedizin*, 1974, **33**(4), 285–295.

14 **Brammer, A. J.** and **Pyykko, I.** Vibration-induced neuropathy. Detection by nerve conduction measurements. *Scand. J. Work, Environment Health*, 1987, **13**(4), 317–322.

15 **Chang, K. Y., Ho, S. T.,** and **Yu, H. S.** Vibration induced neurophysiological and electron microscopical changes in rat peripheral nerves. *Occup. Environ. Medicine*, 1994, **51**(2), 130–135.

16 **Curry, B. D., Bain, J. L., Yan, J. G., Zhang, L. L., Yamaguchi, M., Matloub, H. S.,** and **Riley, D. A.** Vibration injury damages arterial endothelial cells. *Muscle Nerve*, 2002, **25**(4), 527–534.

17 **Necking, L. E., Dahlin, L. B., Friden, J., Lundborg, G., Lundstrom, R.,** and **Thornell, L. E.** Vibration-induced muscle injury. An experimental model and preliminary findings. *J. Hand Surg. Br.*, 1992, **17**(3), 270–274.

18 **Krajnak, K., Waugh, S., Wirth, O.,** and **Kashon, M. L.** Acute vibration reduces Aβ nerve fiber sensitivity and alters gene expression in the ventral tail nerves of rats. *Muscle Nerve*, 2007, **36**(2), 197–205.

19 **Krajnak, K., Dong, R. G., Flavahan, S., Welcome, D. E.,** and **Flavahan, N. A.** Acute vibration increases $\alpha_{2c}$-adrenergic smooth muscle constriction and alters thermosensitivity of cutaneous arteries. *J. Appl. Physiology*, 2006, **100**, 1230–1237.

20 **Dong, R. G., McDowell, T. W., Welcome, D. E.,** and **Wu, J. Z.** Biodynamic response of human fingers in a power grip subjected to a random vibration. *J. Biomech. Engng*, 2004, **126**, 446–456.

21 **Kihlberg, S.** Biodynamic response of the hand-arm system to vibration from an impact hammer and a grinder. *Int. J. Ind. Ergonomics*, 1995, **16**, 1–8.

22 **Reynolds, D.** and **Angevine, E. N.** Hand–arm vibration part II: vibration transmission characteristics of the hand and arm. *J. Sound Vibr.*, 1977, **51**, 255–265.

23 **Dong, J. H., Dong, R. G., Rakheja, S., Welcome, D. E., McDowell, T. W.,** and **Wu, J. Z.** A method for analyzing absorbed power distribution in the hand and arm substructures when operating vibrating tools. *J. Sound Vibr.*, 2008, **311**, 1286–1309.

24 **Wu, J. Z., Welcome, D. E., Krajnak, K.,** and **Dong, R. G.** Finite element analysis of the penetrations of shear and normal vibrations into the soft tissues in a fingertip. *Med. Engng Physics*, 2007, **29**(6), 718–727.

25 **Dong, R. G., Schopper, A. W., McDowell, T. W., Welcome, D. E., Wu, J. Z., Smutz, W. P., Warren, C.,** and **Rakheja, S.** Vibration energy absorption (VEA) in human fingers-hand-arm system. *Med. Engng Physics*, 2004, **26**(6), 483–492.

26 **Dong, R. G., Welcome, D. E., McDowell, T. W., Wu, J. Z.,** and **Schopper, A. W.** Frequency weighting derived from power absorption of fingers-hand-arm system under $z_h$-axis. *J. Biomechanics*, 2006, **39**, 2311–2324.

27 **Bystrom, S.** and **Fransson-Hall, C.** Acceptability of intermittent handgrip contractions based on physiological response. *Human Factors*, 1994, **36**(1), 158–171.

28 **Farkkila, M.** and **Pyykko, I.** Blood flow in the contralateral hand during vibration and hand grip contractions of lumberjacks. *Scand. J. Work, Environment Health*, 1979, **5**(4), 368–374.


## APPENDIX

### Notation

| | |
|---|---|
| $A_i$ | tail acceleration at the $i$th index (A, B, C, D, E, F, G, H, I, J, K, L, and M) (see Fig. 1) ($m/s^2$) |
| $A_{ref}$ | acceleration at the reference point ($m/s^2$) |

| | |
|---|---|
| $c_{Tail}$ | tail viscous damping per unit length ((N s/m)/m) |
| DOF | degree of freedom |
| $k_{Tail}$ | tail effective contact stiffness (N/m) |
| $M_{Tail}$ | effective mass of tail in the mechanical (kg) |
| $p$ | probability |
| $P_{Tail}$ | power absorbed in each unit length of the tail (W) |
| $T_r$ | transmissibility |
| $W_{Tail}$ | frequency weighting of the tail's vibration power absorption |
| $\Delta D_{Tail}$ | relative displacement between tail equivalent mass and the vibrating plate (mm) |
| $\omega$ | vibration frequency (rad/s) |